

Electrically Assisted Magnetic Recording in Multiferroic Nanostructures

F. Zavaliche,* T. Zhao, H. Zheng, F. Straub, M. P. Cruz,† P.-L. Yang, D. Hao, and R. Ramesh

Department of Materials Science and Engineering, and Department of Physics, University of California Berkeley, Berkeley, California 94720

Received February 26, 2007; Revised Manuscript Received April 24, 2007

ABSTRACT

We demonstrate the room-temperature control of magnetization reversal with an electric field in an epitaxial nanostructure consisting of ferrimagnetic nanopillars embedded in a ferroelectric matrix. This was achieved by combining a weak, uniform magnetic field with the switching electric field to selectively switch pillars with only one magnetic configuration. On the basis of these experimental results, we propose to use an electric field to assist magnetic recording in multiferroic systems with high perpendicular magnetic anisotropy.

As the bit size in magnetic data storage approaches the superparamagnetic limit, increasing the magnetic anisotropy is needed to ensure bit stability, which in turn requires an undesirable strong switching field. To enable magnetic recording with a weak field, heat from a focused laser beam was used to locally decrease the anisotropy in what is known as heat-assisted magnetic recording (HAMR).¹ In this work, we propose an alternative way to enable low-field magnetic recording in high-anisotropy media with electric field. Such a typical media is a multiferroic nanostructure with matrix-pillar morphology,^{2–5} which exhibits strong magnetoelectric coupling^{5–8} to enable the electrically assisted magnetic recording (EAMR). From the basic science standpoint, our data proves that the electric-field-induced magnetization reversal process can be made controllable in multiferroic nanostructures with perpendicular magnetic anisotropy by applying a weak magnetic field. In zero magnetic field, the effect is stochastic.

The multiferroic nanostructure used in this work is a 300 nm thick epitaxial film with composition $(\text{BiFeO}_3)_{0.65}(\text{CoFe}_2\text{O}_4)_{0.35}$ grown by pulsed laser deposition at ~ 700 °C on SrRuO₃-buffered SrTiO₃(001). The magnetic hysteresis loops have been acquired with a vibrating sample magnetometer. Magnetic force microscopy (MFM, phase detection) in the tapping-lift mode was used to image the magnetic domains. The magnetic probe was magnetized in the up direction, and consequently, the down-magnetized pillars appear white in our MFM images (repulsive probe-film interaction), while the up-magnetized pillars appear black (attractive interaction). To locally pole the film, a constant bias was applied to a conducting, Pt-coated atomic force

microscopy (AFM) probe during scanning in contact mode. All scans in this work have been performed at room temperature in air.

An atomic force microscopy (AFM) scan of the multiferroic BiFeO₃–CoFe₂O₄ nanostructure investigated here is shown in Figure 1a. The faceted⁴ rectangular CoFe₂O₄ nanopillars embedded in BiFeO₃ can be clearly seen. Transmission electron microscopy images (not shown here) confirm the pillar-matrix morphology. Particle analysis performed on the AFM images gives a mean size of 92 nm with a standard deviation of 27 nm. Therefore, the nanopillars in this film exhibit an aspect ratio of $\sim 1:3$ (lateral size: height). The magnetic hysteresis loops indicate a perpendicular magnetic anisotropy (Figure 1b), originating from a combination of nanopillar shape and heteroepitaxial stresses imposed by the epitaxial matrix.

To verify that this nanostructure shows a strong magnetoelectric coupling, the film was first magnetized either up or down and then electrically poled. The change of nanopillars magnetization following the matrix ferroelectric switching^{5,9} was imaged by MFM. Placing the sample in 20 kOe perpendicular fields yields a uniform out-of-plane pillar magnetization, as one can see in the MFM images shown in Figure 1c (down magnetization) and Figure 1d (up magnetization). This uniform magnetic contrast suggests that the ferrimagnetic nanopillars are predominantly in a single domain state, although the average lateral pillar size is larger than the critical size for single domain CoFe₂O₄, i.e., ~ 70 nm.¹⁰ This may be attributed to the observed uniaxial magnetic anisotropy (Figure 1b). After the MFM scans in Figure 1c,d were taken, the magnetic probe was replaced with a conducting nonmagnetic one, and the ferroelectric BiFeO₃ matrix was electrically poled in the areas outlined in Figure 1c,d at a tip bias of -16 V. The MFM images

* Corresponding author. E-mail: florin.zavaliche@seagate.com.

† Universidad Nacional Autónoma de México, Centro de Ciencias de la Materia Condensada, Km 107 Carretera Tijuana-Ensenada, Ensenada B.C., México C.P. 22800.

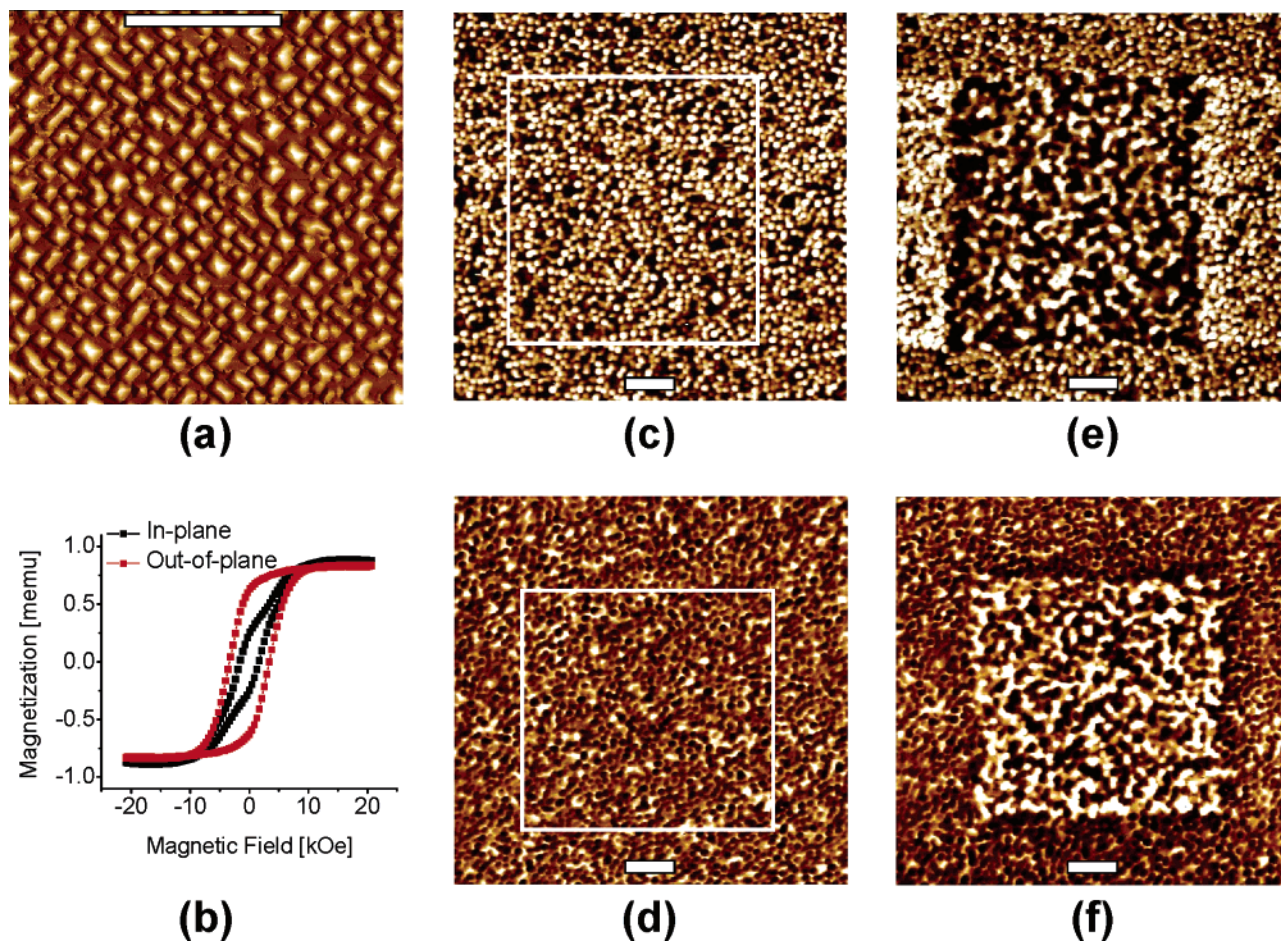


Figure 1. Morphology and magnetization switching in the $(\text{BiFeO}_3)_{0.65}-(\text{CoFe}_2\text{O}_4)_{0.35}$ nanostructure. (a) Surface topography as seen by AFM. (b) Out-of-plane (red symbols) and in-plane (black symbols) magnetization loops. (c,d) MFM scans after magnetization in down and up 20 kOe fields, respectively. (e,f) MFM scans taken in the same areas as in (c) and (d), respectively, after electrical poling at -16 V. The bars are $1 \mu\text{m}$.

acquired after electrical poling (Figure 1e,f) reveal dramatic changes in the magnetic configuration in many nanopillars, mainly due to magnetization reversal (full contrast reversal) rather than forming magnetic domains or flipping to an in-plane direction, as we reported earlier.⁵ The change in contrast outside the poled area in Figure 1e is an artifact induced by flattening the raw MFM image. Obviously, the electric field-induced magnetization switching process is influenced by the pillars' lateral size and aspect ratio, which in turn dictate the magnitude of strain-induced and shape magnetic anisotropies.

Thus, it is clear that such $\text{BiFeO}_3-\text{CoFe}_2\text{O}_4$ multiferroic nanostructures exhibit a strong magnetoelectric coupling at room temperature. Here, this effect manifests as the reversal of magnetization upon the application of an electric field, as seen in Figure 1e,f. The magnetic polarization switches following the ferroelectric switching for both the parallel and antiparallel orientation between them. Area analysis performed on the images shown in Figure 1e,f gives a reversal fraction of about $50 \pm 10\%$ in both cases, as independently verified by magnetic dichroism experiments.¹¹ This is in agreement with the mechanism of stress-mediated coupling between the ferroelectric matrix and ferrimagnetic nanopillars,⁵ as discussed in the following and schematically

depicted in Figure 2. An initial state with perpendicular magnetic anisotropy and up magnetization is sketched in Figure 2a. As the BiFeO_3 matrix goes through a pseudocubic phase transition during switching (Figure 2b), the compressive stress reaches a maximum. Because of the intimate contact between the two ferroic components, this compressive stress is transferred to the highly magnetostrictive CoFe_2O_4 nanopillars ($\lambda_{100} = -350 \times 10^{-6}$). Consequently, the nanopillars exhibit an increased perpendicular magnetic anisotropy. After the matrix ferroelectric polarization switches, the nanopillars experience a tensile stress because the applied bias is significantly higher than the coercive voltage of BiFeO_3 (~ 5 V). Given the negative nanopillars' magnetostriction, one would expect that most of them will undergo a transient change of the perpendicular magnetic anisotropy (proved later in the paper), as in multilayer systems.^{12,13} For a short time, a fourfold in-plane magnetic anisotropy takes over, and a spin reorientation transition from out-of-plane to in-plane may occur (Figure 2c) to minimize the anisotropy energy. As the tensile piezostress is relieved following the removal of the applied bias, the initial out-of-plane magnetic anisotropy takes over and magnetization may flip either up or down with equal probabilities (Figure 2d). In this picture, coupling lacks directionality, and about 50% of pillars reverse

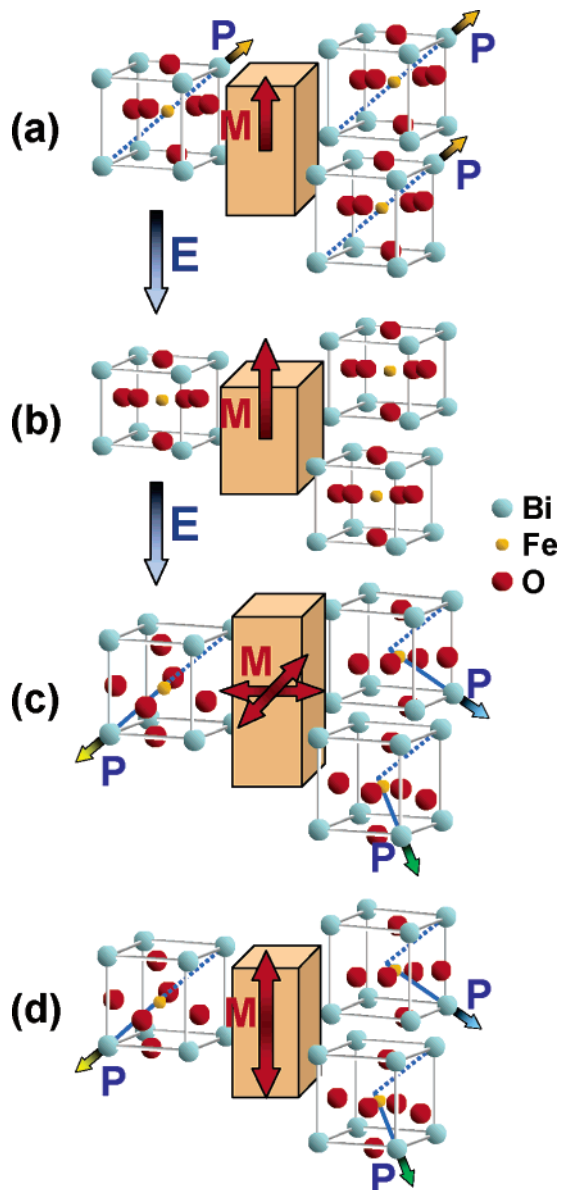


Figure 2. Sketch of magnetization reversal process in CoFe_2O_4 due to polarization switching in the BiFeO_3 matrix following the application of an electric field. (a) Initial configuration with perpendicular magnetic anisotropy, (b) increased perpendicular magnetic anisotropy due to the compressive stress following the spontaneous distortion in the matrix, (c) fourfold in-plane magnetic anisotropy induced by the tensile piezoelectric deformation in the matrix, and (d) final configuration with perpendicular magnetic anisotropy. The three possible ferroelectric switching mechanisms (ref 9) responsible for coupling are depicted along with the atomic structure of BiFeO_3 .

magnetization, in very good agreement with the experimental results depicted in Figure 1c–f. A close inspection of the MFM images in Figure 1e,f points at some degree of collective switching, which may be a result of a finite exchange interaction between pillars. This may occur if several pillars are touching one another, as inferred by the topographic image in Figure 1a.

If this is the mechanism responsible for magnetoelectric coupling in our nanostructure, then applying a sufficiently high bias with opposite polarity (ferroelectric nonswitching

conditions) should produce a similar effect. This is because only the steps depicted in Figure 2c,d lead to the switching of magnetization. Indeed, a bias of +16 V applied as before was able to reverse the magnetization in about 30% of the nanopillars in the scanned area (not shown). The lower reversal percentage measured for the positive applied bias (nonswitching ferroelectric polarization) may be the result of a less favorable stress dynamics, i.e., energetics, than under ferroelectric switching conditions.

To support the validity of the above mechanism, we estimated the stress along the z -direction produced by the tensile piezodeformation in BiFeO_3 under our experimental conditions and found a value of ~ 0.6 GPa. This stress is transferred through the BiFeO_3 – CoFe_2O_4 interface and produces a magnetoelastic energy in the nanopillars of density $\sim 3.2 \times 10^5$ J/m³. If magnetoelectric coupling exists, this value must be larger than the sum of energy terms associated with the pillars' shape, heteroepitaxial-induced stresses and intrinsic magnetocrystalline anisotropy ($K_1 \approx 2 \times 10^5$ J/m³). Estimates of the first two contributions were calculated as 0.2×10^5 and 1×10^5 J/m³, respectively. Although fragile, the energy balance tells us that the magnetic anisotropy and/or coercivity can be altered in an epitaxial ferroelectric–ferrimagnetic nanostructure with large enough spontaneous distortion and high magnetostriction. Detailed calculations that consider the different ferroelectric switching mechanisms in BiFeO_3 ⁹ may be able to account for the different reversal rates for switching and nonswitching bias conditions.

We demonstrate now the concept of electrically assisted magnetic recording (EAMR) in a multiferroic nanostructure. To do so, dc magnetic fields much weaker than the out-of-plane coercive field (3.5 kOe, see Figure 1b) have been applied along film's normal direction during the *whole* experiment (MFM–electrical poling–MFM) and over the *whole* sample, as sketched in Figure 3a. The field direction was chosen to favor MFM probe's magnetization, i.e., pointing up. Shown in Figure 3b–e are the results obtained in a 700 Oe field for the two initial pillars' magnetic states: down (Figure 3b,c) and up (Figure 3d,e). The electric field was applied as before in the outlined areas. In the case of down-magnetized films, the weak up uniform magnetic field was able to switch almost all nanopillars, but only in the electrically poled area (Figure 3c). This also proves the inference we made above that most of the nano pillars undergo a transient change of their built-in magnetic anisotropy in an applied electric field.

In contrast, for the up-magnetized film, the weak magnetic field favors the nanopillars' magnetic state and electrical poling performed under the same conditions as before induces little changes (Figure 3e). Consequently, although the application of an electric field alters the magnetic anisotropy, the dipolar or Zeeman term ($-HM \cos \varphi$) of magnitude $\sim 1 \times 10^5$ J/m³ may hinder magnetization rotation. In this expression, φ is the angle between nanopillars magnetization, M , and the applied magnetic field, H .

Beside the working principle of EAMR, the results shown here prove that one may control the electric field-induced

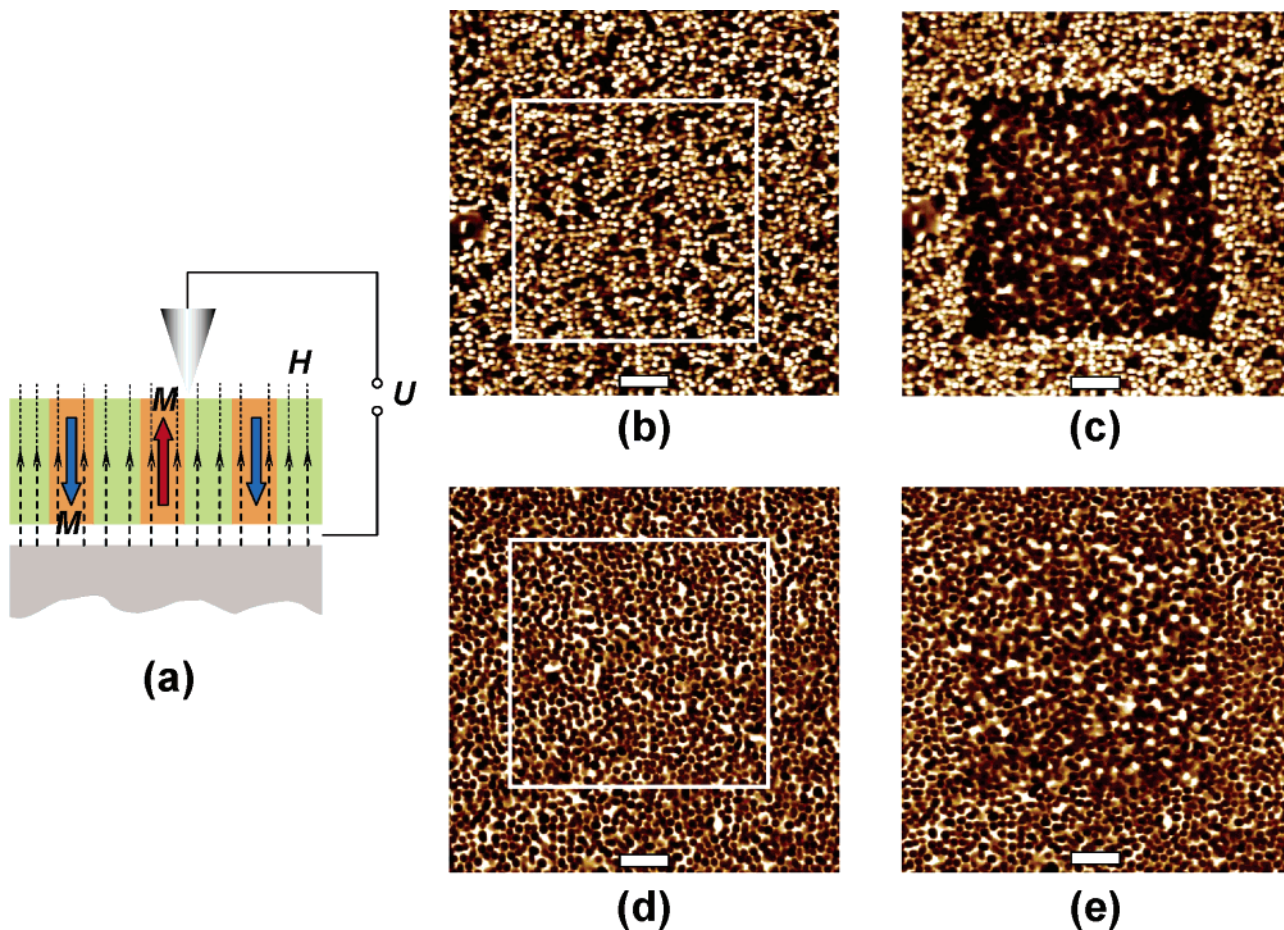


Figure 3. The principle of EAMR in $(\text{BiFeO}_3)_{0.65}-(\text{CoFe}_2\text{O}_4)_{0.35}$ multiferroic nanostructure. (a) Sketch of the experimental setup. (b) MFM after magnetization in a down 20 kOe field before and (c) after poling at -16 V in a 700 Oe up-magnetic field. (d) MFM after magnetization in an up 20 kOe field before and (e) after poling at -16 V in a 700 Oe up-magnetic field. The bars are $1 \mu\text{m}$.

magnetization reversal by changing the direction of either magnetization or the bias magnetic field. Area analysis gives a reversal percentage of 25 and $75 \pm 5\%$ at -16 V/700 Oe for the up- and down-magnetized films, respectively. Therefore, the application of a weak, uniform perpendicular magnetic field during electrical poling renders directionality and control to the magnetoelectric coupling effect. Moreover, these results prove that a strong magnetoelectric coupling exists between most of the nanopillars and matrix.

To find the optimum conditions for EAMR in our nanostructure, we carried out field-dependent magnetoelectric coupling experiments (Figure 4a,b). Except for the out-of-plane magnetization data in Figure 4a (triangles), which were taken from Figure 1c and normalized to remanence, each data point in Figure 4 corresponds to distinct switching experiments. The error bars reflect the accuracy in determining the switched area from the MFM images. The data shown in Figure 4a were obtained in up-magnetic fields for both up (open squares) and down (solid squares) pillars magnetization. The ferroelectric matrix was switched at -16 V. At fields up to ~ 600 Oe, a slight increase in the amount of switched magnetic nanopillars was measured at -16 V for the down-magnetized film (solid squares in Figure 4a) with respect to the case of zero magnetic field. For the up-magnetized film (open squares in Figure 4a), the amount of

switched pillars is slightly reduced. As the magnetic field is increased, a steep increase in the switched area was measured for the down-magnetized pillars at -16 V, while the switching of up-magnetized pillars is suppressed. Therefore, the combination of a weak magnetic field with the electric field leads to the preferential switching of pillars with a certain perpendicular magnetic state. In our view, the slope and shape of the curves in Figure 4a reflect the nanopillar size distribution and morphology,^{14,15} as well as the gradual alteration of the energy balance calculated above with the addition of the Zeeman term. The abrupt change in the amount of nanopillars reversing their magnetization in a constant electric field with increasing the magnetic field is in sharp contrast to the slow changing magnetization in zero electric field (triangles in Figure 4a).

Finally, the electric bias dependence of the switched magnetic area is shown in Figure 4b. A 580 Oe magnetic field was combined with the electric bias to improve the accuracy of switched area determination at low electric fields. The electrically switched magnetic area decreases gradually at poling biases below -14 V and vanishes close to the ferroelectric coercive voltage. This result suggests that the piezoelectric deformation induced by the different ferroelectric/ferroelastic switching mechanisms plays an important role in EAMR.

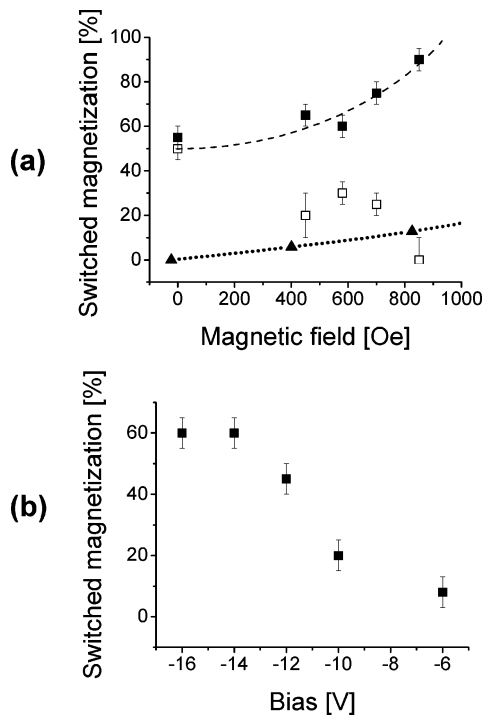


Figure 4. Field dependence of the reversed magnetic area by an applied electric field. (a) magnetic field dependence at -16 V for up- (open squares) and down-magnetized (solid squares) films. The magnetic field was applied perpendicular to the films in the up direction. Plotted with solid triangles are normalized out-of-plane magnetization data at zero electric field from Figure 2b. The curves are guides to the eye. (b) Electrical bias dependence at 580 Oe for down-magnetized film.

In conclusion, by optimizing the growth of $(\text{BiFeO}_3)\text{--}(\text{CoFe}_2\text{O}_4)$ heterostructures, we synthesized multiferroic film nanostructures exhibiting two electrically switchable perpendicular magnetic states at ambient conditions. This work demonstrates for the first time the working principle of EAMR. Moreover, the magnetoelectric coupling effect becomes controllable in a weak perpendicular magnetic field. In our view, using such materials as recording media has a threefold advantage. First, as in the HAMR approach, no

electrical currents are involved in softening the magnetic medium, resulting in a low power consumption. Second, the electric field can be easily confined around individual bits, ensuring high resolution. Third, the bits are very sharp and stable because they are physically defined as individual magnetic nanopillars in a nonmagnetic (ferroelectric) matrix. Further reduction of pillar diameter well below ~ 90 nm, together with a good separation between pillars, must be achieved to facilitate the technical feasibility of the recording scheme we proposed in this letter.

Acknowledgment. This work has been supported by ONR under grant no. N00014-06-1-0008, MURI grant no. E-21-6RU-G4, and ARO under Prime award no. W911NF-04-1-247.

References

- (1) McDaniel, T. W. *J. Phys.: Condens. Matter* **2005**, *17*, R315.
- (2) Zheng, H.; Wang, J.; Lofland, S. E.; Ma, Z.; Mohaddes-Ardabili, L.; Zhao, T.; Salamanca-Riba, L.; Shinde, S. R.; Ogale, S. B.; Bai, F.; Viehland, D.; Jia, Y.; Schlom, D. G.; Wuttig, M.; Roytburd, A.; Ramesh, R. *Science* **2004**, *303*, 661.
- (3) Li, J.; Levin, I.; Slutsker, J.; Provenzano, V.; Schenck, P. K.; Ramesh, R.; Ouyang, J.; Roytburd, A. L. *Appl. Phys. Lett.* **2005**, *87*, 072909.
- (4) Zheng, H.; Zhan, Q.; Zavaliche, F.; Sherburne, M.; Straub, F.; Cruz, M. P.; Chen, L. Q.; Dahmen, U.; Ramesh, R. *Nano Lett.* **2006**, *6*, 1401.
- (5) Zavaliche, F.; Zheng, H.; Mohaddes-Ardabili, L.; Yang, S. Y.; Zhan, Q.; Shafer, P.; Reilly, E.; Chopdekar, R.; Jia, Y.; Wright, P.; Schlom, D. G.; Suzuki, Y.; Ramesh, R. *Nano Lett.* **2005**, *5*, 1793.
- (6) Spaldin, N. A.; Fiebig, M. *Science* **2005**, *309*, 391.
- (7) Fiebig, M. *J. Phys. D: Appl. Phys.* **2005**, *38*, R123.
- (8) Eerenstein, W.; Mathur, N. D.; Scott, J. F. *Nature* **2006**, *442*, 759.
- (9) Zavaliche, F.; Shafer, P.; Ramesh, R.; Cruz, M. P.; Das, R. R.; Kim, D. M.; Eom, C. B. *Appl. Phys. Lett.* **2005**, *87*, 252902.
- (10) Berkowitz, A.; Schuele, W. J. *J. Appl. Phys.* **1959**, *30*, S134.
- (11) Zhao, T.; Scholl, A.; Zavaliche, F.; Zheng, H.; Barry, M.; Doran, A.; Lee, K.; Cruz, M. P.; Ramesh, R. *Appl. Phys. Lett.* **2007**, *90*, 123104.
- (12) Iwasaki, Y. *J. Magn. Magn. Mater.* **2002**, *240*, 395.
- (13) Kim, S.-K.; Lee, J.-W.; Shin, S.-C.; Song, H. W.; Lee, C. H.; No, K. *J. Magn. Magn. Mater.* **2003**, *267*, 127.
- (14) Levin, I.; Li, J.; Slutsker, J.; Roytburd, A. L. *Adv. Mater.* **2006**, *18*, 2044.
- (15) Zheng, H.; Straub, F.; Zhan, Q.; Yang, P. L.; Hsieh, W.-K.; Zavaliche, F.; Chu, Y.-H.; Dahmen, U.; Ramesh, R. *Adv. Mater.* **2006**, *18*, 2747.

NL0704650